



# The effect of simultaneous heat/fire and impact on carbon fibril and particle release from carbon fiber-reinforced composites

Robert Chapple, Baljinder Kandola, Peter Myler, Laurent Ferry, J. Lopez-Cuesta, Carine Chivas-joly, Emmajane Erskine

## ► To cite this version:

Robert Chapple, Baljinder Kandola, Peter Myler, Laurent Ferry, J. Lopez-Cuesta, et al.. The effect of simultaneous heat/fire and impact on carbon fibril and particle release from carbon fiber-reinforced composites. *Polymer Composites*, 2021, 42 (11), pp.6127-6145. 10.1002/pc.26290 . hal-03338732

**HAL Id: hal-03338732**

**<https://imt-mines-ales.hal.science/hal-03338732>**

Submitted on 23 Nov 2021

**HAL** is a multi-disciplinary open access archive for the deposit and dissemination of scientific research documents, whether they are published or not. The documents may come from teaching and research institutions in France or abroad, or from public or private research centers.

L'archive ouverte pluridisciplinaire **HAL**, est destinée au dépôt et à la diffusion de documents scientifiques de niveau recherche, publiés ou non, émanant des établissements d'enseignement et de recherche français ou étrangers, des laboratoires publics ou privés.

# The effect of simultaneous heat/fire and impact on carbon fibril and particle release from carbon fiber-reinforced composites

Robert Chapple<sup>1</sup>      Baljinder K. Kandola<sup>1</sup>      Peter Myler<sup>1</sup>  
Laurent Ferry<sup>2</sup>      José-Marie Lopez-Cuesta<sup>2</sup>      Carine Chivas-Joly<sup>3</sup>  
Emmajane L. Erskine<sup>4</sup>

<sup>1</sup>Institute for Materials Research and Innovation, University of Bolton, Deane Road, Bolton, UK

<sup>2</sup>Polymers Composites and Hybrids (PCH), IMT Mines Ales, 6 Avenue de Clavières, Alès Cedex, France

<sup>3</sup>Laboratoire National de Métrologie et D'essais, CARMEN Platform, DMSI, 29 Avenue Roger Hennequin, Trappes, France

<sup>4</sup>Defence Science and Technology Laboratory, Porton Down, Salisbury, UK

## Correspondence

Baljinder K. Kandola, Institute for Materials Research and Innovation, University of Bolton, Deane Road, Bolton BL3 5AB, UK.  
Email: b.kandola@bolton.ac.uk

## Funding information

Defence Science and Technology Laboratory, Ministry of Defence, UK

## Abstract

A novel laboratory scale testing equipment has been designed and developed, which combines impact and heat/fire conditions to enable the testing of composite laminates, including the ability to capture debris/particles released during the test. This incorporates a pendulum impactor to create impact whilst the sample is exposed to a cone heater at a particular heat flux for a specified period of time. A protocol for testing samples under different conditions and capturing particles released, both from the front and back faces, along with effluents has been provided. A carbon fiber-reinforced epoxy composite was impacted whilst being exposed to different heat fluxes for a range of time periods. A loss of stiffness related to the heating exposure time was found to affect the damage type. At lower heat fluxes, the captured particles included broken carbon fibers, decomposed resinous particles and resin coated fibers. Quantitative and morphological analyses of captured particles demonstrated that the sizes of decomposed resin particles and fibers reduced with longer exposure time or increased heat flux. This information could be useful to provide insight into potential health hazards of components of the composites.

## KEYWORDS

carbon fiber, high-temperature properties, impact behavior, mechanical testing, particles release

## 1 | INTRODUCTION

Carbon fiber-reinforced epoxy composites (CFRC) are most popular in structural applications owing to the high tensile strength and stiffness of carbon fibers. However, out-of-plane impact forces are a major design concern since carbon fiber's impact resistance is lower than other reinforcing fibers such as glass. Unlike metals, carbon fiber composites are susceptible to surface and internal damage. The internal damage under the surface is harder

to inspect, but degrades the mechanical property of the structure and may lead to a sudden failure when the materials are in service.<sup>[1]</sup> Major damage modes include matrix cracking, fiber/matrix debonding, delamination, inter-laminar failure and fiber breakage.<sup>[1–3]</sup> Moreover, due to the brittle nature of epoxy matrix, the overall impact resistance of the composite is lower than other structural materials,<sup>[4]</sup> including carbon fiber reinforced thermoplastic composites.<sup>[5–7]</sup> Quite often thermoplastic polymers such as

polyethersulphone are added in the epoxy resin to improve its toughness.

Due to the increased usage of the CFRCs in aerospace, where the threat of impact by foreign objects is high, extensive research has been carried out on various scenarios of impact and resultant damage evaluation in terms of damage tolerance, crack propagation, and so forth.<sup>[2,8–11]</sup> Various predictive models have also been developed,<sup>[12–15]</sup> which can aid engineers to design suitable carbon fiber architectures to improve damage tolerance.

All polymeric composites, including those which are epoxy based are susceptible to heat-induced damage resulting in significant deterioration in their mechanical properties during and after thermal exposure.<sup>[16–21]</sup> Composites start losing their structural performance when exposed to temperatures above their glass transition temperatures (80°C–130°C, depending on the epoxy resin type) due to the thermal softening of the resin matrices,<sup>[17]</sup> while at temperatures higher than 300°C, the resin starts decomposing into volatile gasses and/or solid char.<sup>[16–23]</sup> The degradation of the resin matrix, whose primary function is to constrain the reinforcing fibers, leads to inefficient load transfer between the matrix and the fibers causing significant losses in the structural performance of the composite structure. Most of the research on structural performance of composites in fire has been predominantly performed on glass fiber composites under compression or flexural<sup>[16–21,23]</sup> load, where the dominant mechanism controlling the structural integrity in fire is the thermal softening/decomposition of the polymer matrix. The only available reference for the post-fire impact resistance of glass fiber epoxy composites is by Reis et al.<sup>[24]</sup> In all cases the mechanical properties rapidly reduced with increasing heat flux or heat exposure time.

The response of carbon fiber composites to heat and/or fire in the compression and impact modes would be similar to respective glass fiber composites, these being matrix dominant properties, the impact behavior of the two however, can be very different. There is not much literature available for impact behavior of CFRC during or post fire exposure, though there are some papers on composites exposed to maximum 150°C,<sup>[25,26]</sup> they report that the impact-induced delamination area decreased as the temperature increased. This temperature is below the decomposition temperature of the resin; hence, the observed changes are only due to matrix softening. Another difference between glass and carbon fibers composites is that at higher temperatures and on ignition when the resin burns, glass fibers will melt, whereas carbon fibers could be released into the surroundings. Carbon fibers start oxidizing above 500°C leading to reduction in diameter, reducing further with increasing temperature and prolonged exposure,<sup>[27–29]</sup> becoming more porous and smaller in size. During fire and impact, the broken fibers

after oxidation could defibrillate into fibrils of diameter small enough to be orally inhaled.<sup>[30–33]</sup> There are many reports of aeroplane crashes where rescue team suffered with serious ‘needle-stick’ injuries, respiratory problems, eye and skin irritation, headaches and nausea.<sup>[30,32]</sup> Chemical extraction from air samples taken at aircraft crash sites, which included post-crash fire, showed that large numbers of toxic organic compounds had been absorbed by the fibrous airborne particles.<sup>[33]</sup> In the 1970s the US Naval research organizations and NASA established test programs focused on replicating the impact and fire situations of aeroplane crash in the lab, mainly to capture released carbon fibers. Much of the testing was performed on operational composite aircraft components or large test panels in test scenarios simulating composites in jet fuel fire or impact through explosive charge post propane burner exposure. A test at the NASA’s Ames facility in Redwood City in California, involved the design of combined fire and LVI drop tower equipment, with the ability to capture released fibers post impact.<sup>[34]</sup> The main findings were that overall the collected fibers had a mean diameter  $\sim 4.2\ \mu\text{m}$  versus  $7\ \mu\text{m}$  for the virgin fibers and at extreme flame temperatures ( $>900^\circ\text{C}$ ) and under oxygen-rich test conditions, large amounts of fibers were completely consumed through oxidation. Morrey in 2001<sup>[35]</sup> analyzed fibers retrieved from six crash sites, most of these were of 1–2 mm length and  $3.2\text{--}4.2\ \mu\text{m}$  diameter, which is much smaller than the unburnt fibers ( $6.6\text{--}6.7\ \mu\text{m}$  diameter). In all of these cases the emphasis has been on collection of carbon fibers on exposure to fire only, fire and impact in sequence or samples collected from actual crash sites, where the exact conditions, though realistic, are unquantified. There is a gap in literature for the study on the effect of simultaneous impact and fire on release of carbon fibers as well as any other nano/micro particulates released, which is focus of this study. The work here is primarily concerned with the release of the particles under an impact event at elevated temperatures and identifying the type of debris released and discussing any potential harm that may be caused in such an event. The paper is not concerned with the mechanical performance of the composite after such events as in many cases the material would not be capable of sustaining any useful structural loading.

## 2 | DESIGN AND DEVELOPMENT OF THE NOVEL SIMULTANEOUS IMPACT AND HEAT/FIRE TESTING EQUIPMENT

### 2.1 | Design

To succeed in development of a simultaneous impact and heat/fire test, standard impact testing instruments were

explored, namely a low velocity drop-weight impactor (LVI) and a Charpy pendulum impactor. For heat source, the cone heater from a cone calorimeter instrument<sup>[36]</sup> was used. Prior to fabrication of the equipment, computer-aided design (CAD) schematics were generated to evaluate

design ideas. Three designs were generated and are presented in Figure 1.

*Design 1, low velocity drop-weight impact through cone heater:* The first design as shown in Figure 1A incorporated a radiant cone heater assembly, horizontally fixed

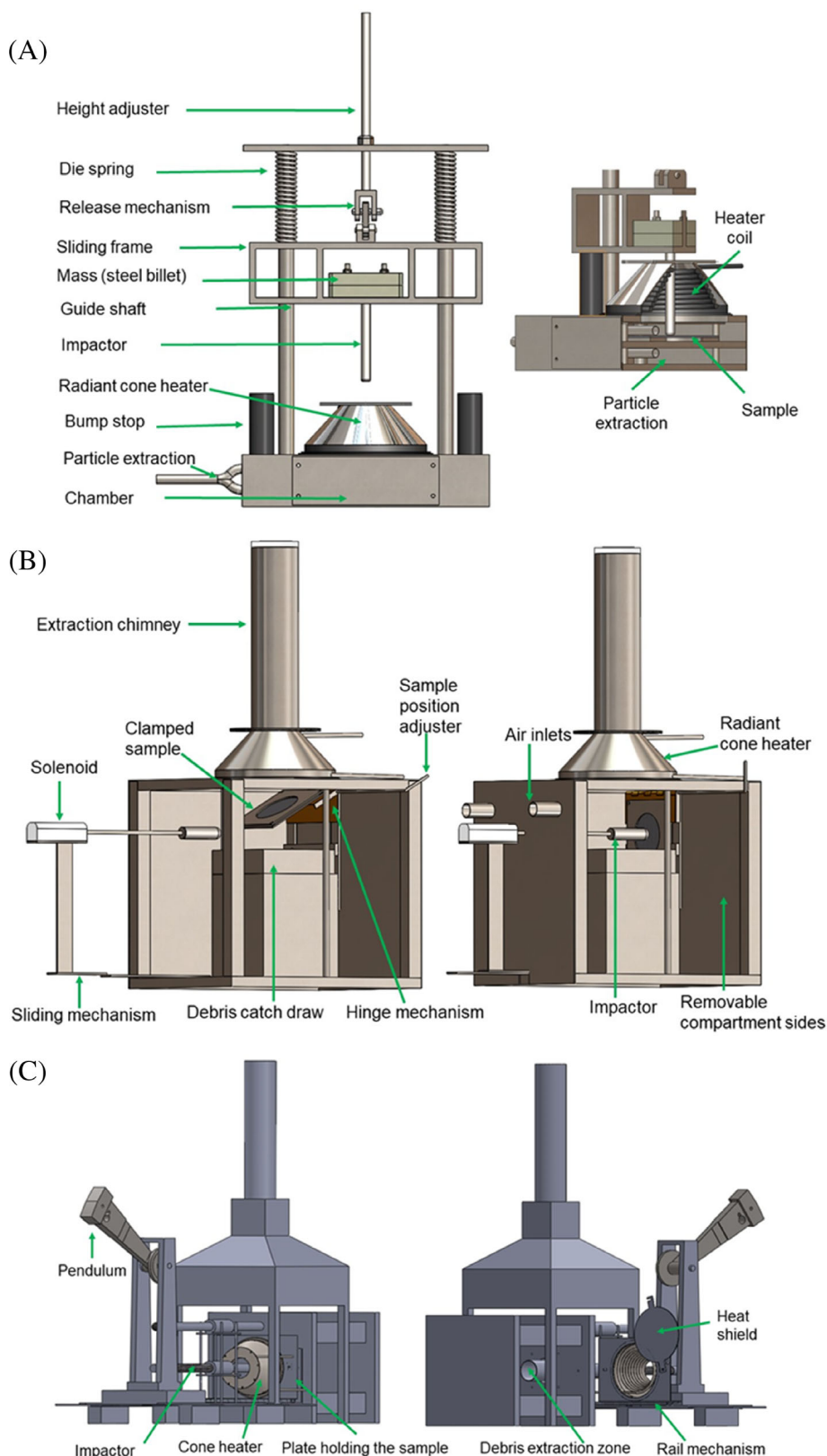


**FIGURE 1** Different CAD designs: (A) design 1; low velocity drop-weight impact through the cone heater, (B) design 2; horizontal impact on a movable, preheated sample under horizontal cone heater and (C) design 3; single pendulum impact on a preheated/ignited sample with a vertical cone heater



above the test area of an LVI. The impactor would travel through the center of the cone heater to impact the test sample during exposure to radiant heat. The impactor would be set at a required height corresponding to desired impact energy. The impact frame, guided on two shafts, connected to a threaded bar, would allow the impact frame height to be increased and so compress two die springs. The implementation of die springs would enable high impact energy within a bench scale frame. In addition, a removable mass could be fitted within the impact frame to further increase impact energy. Once a desired height was set, the impact would be initiated by the release mechanism, and bump stops could be fitted to stop the impact frame colliding with the cone heater if the sample was penetrated. The cone heater assembly would be fitted to a sealed chamber where the sample was clamped in preparation for the impact event. An extraction pipe attached in close proximity to the sample and near to the potential point of damage would extract any debris and particles released during the testing.

*Design 2, horizontal impact on a movable sample:* A second design (Figure 1B) used a controlled-atmosphere cone calorimeter chamber with cone heater. This design featured sample holder plates connected to a hinge mechanism. This would allow the sample to be exposed to the cone heater initially placed in a horizontal location, and then moved to vertical position for the impact. Released debris and particles would then fall into a catch tray, demonstrated in Figure 1B. This method is similar to normal cone calorimetry but with the ability to alter the atmospheric conditions through air or variable oxygen and nitrogen inlets. The impact method for this design would be performed by a shaft traveling horizontally to create the out of plane impact on the vertically secured sample. The shaft would be operated by an electronic, pneumatic or hydraulic solenoid/ram.

*Design 3, pendulum impact:* The third design (Figure 1C) adapted a Hounsfield Balanced Impact Machine (HBIM) to be used as a single pendulum combined with base support from an LVI and a cone heater. The HBIM's original intended use is to induce fracture in a cuboid block in a fixture at the bottom. The device was used to produce the impact energy in a confined space and be portable.

When assessed for functionality, Design 1 turned out to be quite complex. As the experiment was performed in a small sealed unit, to extract released particles efficiently, it would require air to be supplied into the unit so that fire conditions as in ISO 5660 are possible. Moreover, the cone heater when set at high heat flux could possibly destroy the released particles if they contacted its coil, hence particles of interest released during the impact event could be lost.<sup>[35]</sup> Design 2 would overcome the

problem of air flow as it incorporated the atmospheric chamber, however air-borne small ( $<50\text{ }\mu\text{m}$ ) released particles could still be destroyed by the cone heater.<sup>[35]</sup> Moreover, investigation into the capability of impact using various solenoid or rams and guidance from commercial sources, concluded that only moderate impact energies ( $\sim 13\text{ J}$ ) were possible, relative to impractical solenoid / ram piston diameters (320 mm). To damage carbon fiber epoxy samples,  $6.7\text{ J/mm}$  is required<sup>[37]</sup> and this design limits testing to samples with a thickness less than 2 mm. Design 3 (Figure 1C) however, could damage samples up to 3.5 mm thick, had a cone heater design which reduced the potential of destroying released particles due to its vertical orientation. This design had the capability of adding a sealed sampling area at the back face of the sample, an enclosed area at the front face of the sample holder to capture particles, as well as particle sampling in the effluents. This CAD design was used to fabricate the actual prototype of the impact and shaft combination, detailed in the next section.

## 2.2 | Development of the testing equipment

The complete setup developed based on Design 3 (Figure 1C) is shown in Figure 2 with a schematic in Figure 2A. For clarity different parts of the equipment are shown in Figure 3A–G.

### 2.2.1 | Impactor unit and calibration

As shown in Figure 3A, a single pendulum fixed on the base unit was selected, to which different types of impactors could be attached. To ensure the equipment could create sufficient damage to a range of sample thicknesses, provision was made for the pendulum to produce different energy levels, by changing either the pendulum mass or height. Since the maximum possible height is fixed, the corresponding mass had to be increased. To achieve this, two billets of steel were fabricated to the correct size and shape so that they could be mounted to the lower half of the pendulum. With this, 3 mm thick carbon fiber laminates could be completely penetrated. A bump stop was fabricated and mounted to the frame, which allowed the first impact of the shaft but stopped the pendulum's travel so that it could not impact the shaft for a second time. The whole structure was securely braced on a frame to create stiffness and limited movement, the frame also allowed the pendulum to be released from various heights for a desired impact energy.

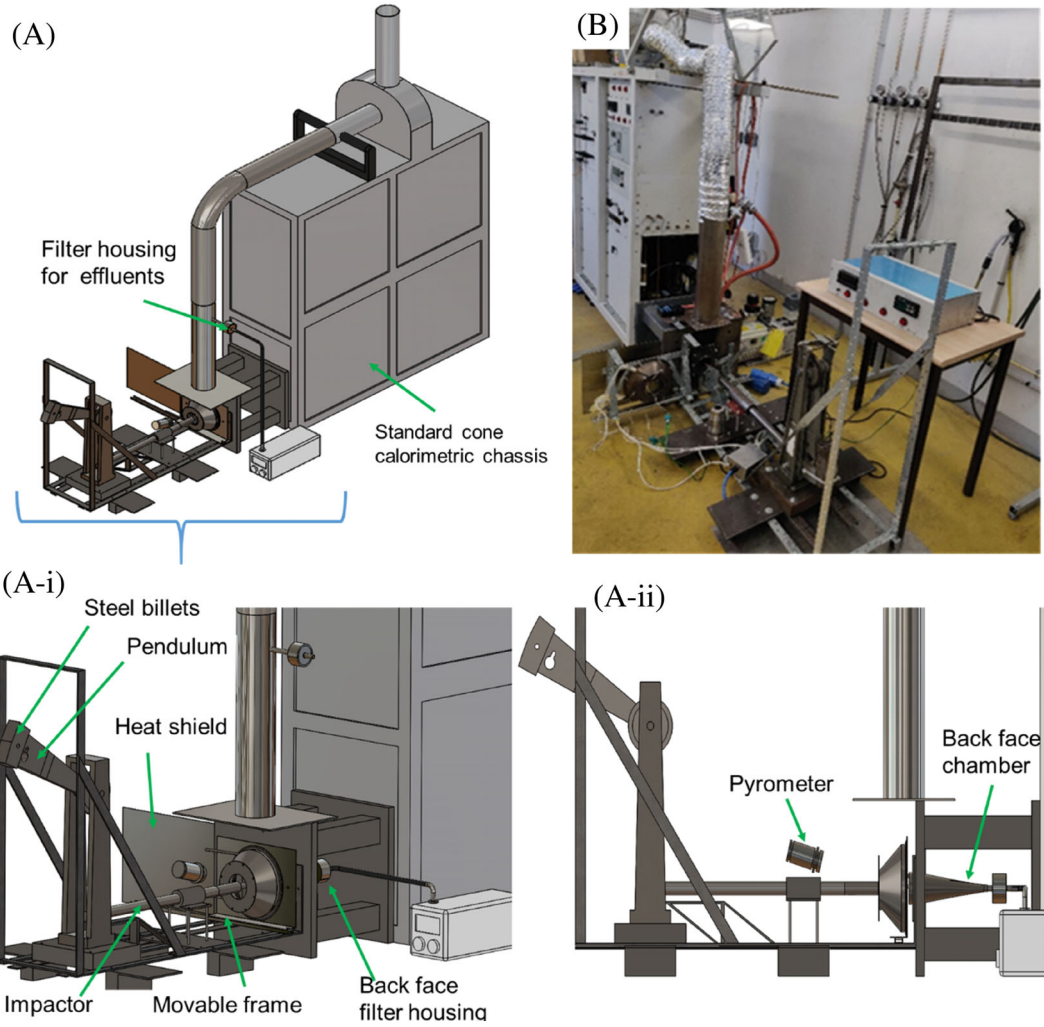


FIGURE 2 Complete setup of the testing equipment: (A) schematic and (B) digital image

From the HBIM pendulum's energy level calibration scale, it could be established that the maximum impact energy from the combined action of the two pendulums as they pass each other was 64 J. The mass of the two pendulums are equal so that they meet in a central location and ensure a balanced impact. Hence, a single pendulum should result in a maximum impact energy of 32 J.

The potential impact energy ( $PE$ ) is dependent on the height ( $h$ ) of the pendulum which in turn is a function of radius ( $r$ ) from the center bearing of the pendulum, its mass ( $m$ ) and angle ( $\theta$ ) measured from the base of the pendulum, presented in Equation (1). However, this provides a theoretical value. The most accurate way to determine the kinetic energy of the pendulum is by direct measurement of its velocity (Equation (2)). If the period of the pendulum, passing between two close positions in its path is measured, then its velocity ( $v_{pend}$ ) can be determined. To take this measurement a magnet was fitted

onto the pendulum, on the plane which was in line with the impact of the shaft. As the magnet passed two electronic sensors that were set at a known distance ( $D_{sen}$ ), the time period ( $T_{sen}$ ), was recorded on an oscilloscope. Using the estimation of pendulum mass, a value for the pendulum kinetic energy was calculated, this value was 25 J.

$$PE = \frac{1}{2}mv^2 = mgh = mgr(1 - \cos(\theta)) \quad (1)$$

$$v_{pend/shaft} = \frac{D_{sen}}{T_{sen}} \quad (2)$$

Testing on three different impactor types was performed for the required calibration. The results are provided in Table 1 and show specific impact energies recorded for each type and the energy transfer rate between pendulum and shaft for each type. The calculated values from these

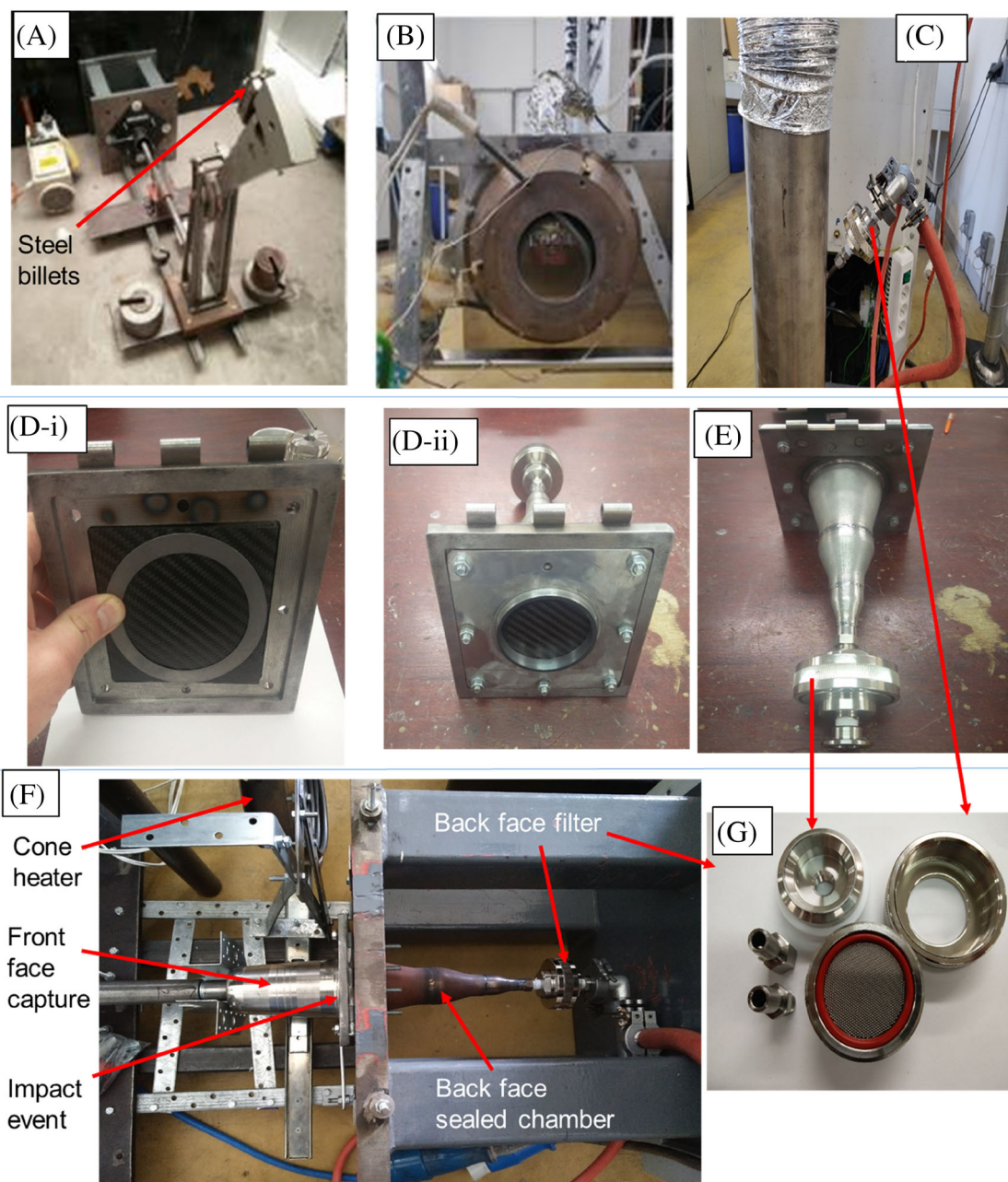





**FIGURE 3** (A) Pendulum impactor on frame, (B) cone heater on a movable frame, (C) Advantec filter housing fitted onto chimney of the cone extraction system (D) i) composite sample fitted into recess of the back plate, ii) sample secured between plates, (E) Advantec filter housing fitted onto back face chamber, (F) complete setup for front and back face particle capture, (G) (E) Advantec LS47 filter housing

velocity measurements are much less than the theoretical values of pendulum potential energy. To determine the height required of the pendulum for the shaft to impact a sample at a specific energy, the percentage of the required impact energy in regards to the maximum possible energy transfer from pendulum to shaft was used. This percentage is used to calculate the resultant height required from the pendulum's maximum impact height. The variation in impact energy between the three impactors is due to their mass. An

increase in impactor shaft mass results in an increase in impact energy. The energy transfer is the difference between the recorded potential energy of the pendulum relative to the impact energy of the shaft. The values correlate to Newton's second law as energy and momentum is conserved during transfer between pendulum and shaft if both objects have the same mass. As the mass of the shaft is increased closer to the pendulum's mass due to impactor type, energy transfer percentage increases.

**TABLE 1** Results of impact energy from each impactor type

Impactor type	Impact energy (J)	Energy transfer (%)
 Small hemispherical	23	92
 Flat	22	88
 Hemispherical	24	96

### 2.2.2 | Sample holder

During testing the composite sample was clamped between two bolted plates. The plate assembly consisted of a front plate and a back plate. The back plate design involved milling two separate depths from a plate of mild steel ( $150 \times 150 \times 10$  mm), seven mounting holes and a 67 mm center hole (Figure 3D [i, ii]) for an open sample back face area. The front plate was also milled from a mild steel plate ( $125 \times 125 \times 3$  mm) to fit precisely into the back plate to create a sealed unit (Figure 3C [i, ii]). A 67 mm center hole and a  $7 \times 3$  mm lip as a front face capture method was also milled from the front face plate. The finished design allows a sample up to  $100 \times 100 \times 3$  mm to be clamped for impact.

Using steel shims between the sample and the plates improves the seal and vacuum increase to greater than 100 mbar was possible. Finally, the back face particle capturing system, comprising three stainless steel concentric reducers, was welded together on to the back plate creating a back face chamber design as shown in Figure 3D.

### 2.2.3 | Cone heater and calibration

A cone heater with a maximum radiant heat flux of  $100 \text{ kW/m}^2$  sourced from Fire Testing Technology Ltd, UK, was fitted into a frame on a sliding rail mechanism (Figure 3B). This design allowed the variable heat exposure and access to the sample. This setup enabled impact to be performed either directly through the center of the cone during fire conditions or impact post-fire conditions once the cone is removed using the rail mechanism. The cone was controlled using an original control unit and power supply from an existing cone calorimeter.

Calibration of the cone was performed by using a heat flux meter connected with the cone heater, set at a distance of 25 mm to the sample face and using extraction of 24 L/s in accordance with the ISO 5660 standard. The impact and fire equipment was connected to the extraction of the standard cone calorimeter demonstrated in Figure 2A,B.

### 2.2.4 | Particle capturing systems from front and back surfaces

An Advantec LS47 stainless steel filter housing (Figure 3G) sourced from Cole-Parmer Instrument Company Ltd was located on to the back face chamber (Figures 2 (i,ii) and 3D) which could be fitted with filters (47 mm diameter) of various mesh sizes. An Edwards RV5 vacuum pump was used for extraction and a Greisinger GDH 200 manometer to monitor the vacuum pressure at the back face during the extraction.

For front face particle capture during impact, a stainless steel cylinder was adapted to allow the impact shaft to pass through it whilst located onto the lip of the front face plate for a semi-sealed environment to hold the particles that are released. This system is shown in Figure 3F. The steel cylinder was not connected to a vacuum system as this over complicated the setup. Particles released during impact were captured in the cylinder and then removed by the rinsing technique described in the following section. It was not possible to use the cylinder in impact during heat / fire conditions tests due to the combination of its design and the necessary location of the radiant cone heater. Instead released particles were collected by rinsing the front face lip with a solvent, as discussed in the following section.



## 2.2.5 | Particle capturing system from effluents

An Advantec LS47 stainless steel filter housing, as used with the back face chamber configuration (Figure 3E) was mounted onto the chimney of a cone extraction system as shown in Figures 2A and 3C along with Greisinger GDH 200 manometer to monitor the vacuum pressure.

## 3 | EXPERIMENTAL

### 3.1 | Materials and composite sample preparation

Carbon Fibers: Torayca T300, 3 K, 0/90° 2 × 2 twill weave, 200 Tex,  $\rho = 1.76 \text{ g/cm}^3$ , filament diameter 7  $\mu\text{m}$ , sourced from SF Composites, Mauguio, France.

Epoxy Resin: Epilok 60–822 resin, diglycidyl ether of bisphenol A/F and Curamine 32–790 NT Hardener, an amine based curing agent, both supplied by Bitrez Ltd, Wigan, UK.

The epoxy resin and curing agent were mixed in the ratio 100:38 by weight and mechanically-stirred for about 5 min. Air bubbles were then removed by degassing in a vacuum chamber. Resin was infused into 10 plies of 300 × 300 mm sized carbon fibers by resin infusion, cured at room temperature for 24 h, followed by post curing in oven at 80°C for 8 h. The fiber weight fraction (FWF) of the samples was 69.3%  $\pm$  1.4% and thickness 2.31 mm  $\pm$  0.04 mm. The composite laminate was cut into samples of sizes 100 × 100 mm by band saw for testing.

### 3.2 | Methodology: Simultaneous impact and heat/fire experiments

The design of the equipment enables many scenarios to be performed. It is possible to impact samples over a range of 1–24 J with the option of multiple different impactor types and sizes. Each value of impact energy combined with each different impactor type will cause different levels of damage to a sample and release different levels and size ranges of particles. A set of experiments was performed with three impactors (Table 1) creating 16–23 J energy. The hemispherical type impactor, set at 19 J, was selected based on this work, with which visible damage occurred on the front and back faces along with good potential for particle generation and capturing.

In addition to these impact scenarios, a range of radiant heat fluxes from 15 to 100 kW/m<sup>2</sup> can be used. Each heat

flux will cause different levels of decomposition of the sample over time, at a high heat flux of 75 kW/m<sup>2</sup> the sample self-ignited and decomposed quickly. At a lower heat flux of 50 kW/m<sup>2</sup> the sample did not ignite and decomposed more slowly. As the sample decomposes, its mechanical properties reduce and the sample loses stiffness, becoming malleable as the polymer matrix transitions from a solid to a range of volatile decomposition products. Here three scenarios, namely impact without heat, with heat for a specified period of time but no ignition (50 kW/m<sup>2</sup> heat flux) and with ignition leading to fire situation (75 kW/m<sup>2</sup> heat flux) are discussed. For each condition the methodology had to be slightly modified as discussed below:

#### 3.2.1 | Test methodology–Impact only

To prepare each test, any apparatus that was in contact with the sample or part of the particle capturing mechanism required cleaning to reduce contamination. Ethanol and paper towel were first used to rinse the apparatus and remove any dirt/contaminants from their surfaces. Next compressed air was used to remove any remaining contaminants and finally ethanol was used to remove any oil residue left from the compressed air.

Three measurements were taken to record the average height, width and length of the sample. Next a fine brush and compressed air was used to loosen any particles / debris on the samples surface from the band saw cutting process. To achieve precise measurements of the sample mass pre and post-test, a Sartorius Quintix 65-1S analytical balance, accurate to 10  $\mu\text{g}$  was used. Due to the sensitivity of measurements to 10  $\mu\text{g}$ , a settling period of 120 min was required pre-test and 60 min post-test. This period was confirmed by monitoring initial samples every 10 min to determine the maximum time required for a stable reading. Finally, the sample was fitted with care into the sample holder plates.

A 47 mm 0.2  $\mu\text{m}$  Millipore polycarbonate filter (Figure 3G) was weighed thrice using a Sartorius Quintix 65-1S analytical balance to ensure an average measurement accurate to 2  $\mu\text{g}$ . This filter was then fitted into the Advantec LS47 housing (Figure 3G) which was then located onto the back face chamber (Figure 3E). A stainless steel cylinder was used to create a sealed front face environment for particle capture, as shown in Figure 3F. Due to the initial mass of this cylinder, accurate gravimetric analysis was not possible; hence the particles were collected by rinsing with Millipore water after the experiment.

Once the cleaning process and mass measurements were complete, the capturing mechanisms were fitted onto the impact and fire testing equipment. The Edwards

RV5 vacuum pump for back face extraction and the Greisinger GDH 200 manometer to measure vacuum pressure were connected. Finally, the pendulum was set to the required height to obtain 19 J impact energy.

To perform tests with consistency a procedure was created. The vacuum was first switched on and the vacuum gauge pressure was measured for 45 s. After the first 30 s, the vacuum pressure was usually stable, and the remaining time was to ensure consistency throughout experiments. At 45 s, the pendulum was released to create the impact event. Vacuum pressure at the back face chamber was recorded pre and post-impact. The vacuum was then terminated 30 s after the impact event.

Post-test, the front face cylinder and front sample holder plate lip were rinsed using Millipore water into a pre-cleaned evaporating dish, and then rinsed directly from the evaporating dish into a sterile polymer specimen container (60 or 120 mL). The sample holder plus filter housing was then carefully removed from the equipment for gravimetric analysis. The back face chamber was also rinsed directly into a 120 mL specimen container, using Millipore water. Finally, the 47 mm 0.2  $\mu\text{m}$  Millipore polycarbonate filter was weighed thrice post-test, using the Sartorius Quintix 65-1S analytical balance and then stored in a sterile polymer petri dish.

### 3.2.2 | Test methodology–Impact during radiant heat conditions

In this test configuration, impact was performed at 90 s, 120 s, 180 s and 240 s exposure times, directly through the center of the cone heater during 50  $\text{kW}/\text{m}^2$  exposure. The following alteration to the impact only test preparation and procedure was made for the inclusion of the radiant heat.

Prior to each test, a sample was weighed using a Sartorius Quintix 124-1S analytical balance which provided a mass measurement accurate to 100  $\mu\text{g}$ . At this resolution, an accurate mass reading was achieved within 1 min; no sample settling time was required. The accuracy of the mass loss to 10  $\mu\text{g}$  during radiant heat exposure was not required as mass was lost during the experiment through effluents and no methodology to measure the effluent mass loss was established in this work.

During impact tests at 90 s, sampling of the effluents (explained in Section 2.2.5) was performed from 30 s before sample exposure to heat source until 30 s after removal of heat source onto 47 mm 0.2  $\mu\text{m}$  Millipore polycarbonate filter (weighed thrice pre and post-test) in the Advantec filter housing (Figure 3G). Impact at 90 s was in attempt to determine if any particulates / fibers could be found in the effluents. At 90 s during 50  $\text{kW}/\text{m}^2$ ;

generally, a large quantity of volatiles were released from the sample and could be visually witnessed. During impact at 120 s, 180 s and 240 s, extraction of particulates, onto a 47 mm diameter, 0.2  $\mu\text{m}$  Millipore polycarbonate filter, from the back face chamber was performed. Sampling began from 30 s pre-impact to 30 s post-impact.

Post experiment the back face chamber was rinsed directly into a 120 mL specimen container with ethanol instead of Millipore water. To remove resin residue containing released particles in the back face chamber, a solvent was required due to the residue's adhesive properties. To sample particles released from the front face, the lip of the front face plate was rinsed into an evaporating bowl with ethanol and then rinsed into a 60 mL polymer specimen container. The polycarbonate filters from the back face or from effluents were weighed and stored in separate sterile polymer petri dishes.

### 3.2.3 | Test methodology–Impact during fire conditions

Radiant heat flux was increased to 75  $\text{kW}/\text{m}^2$  to perform impact during fire conditions. The preparation of the experiments and the collecting of residue and particles at both the front and back face post-test were performed in the same manner as for heat conditions. However, extraction of particulates from the back face chamber was performed after a 20 min cooling period to prevent excessive filter damage and protect the vacuum pump. The back face filter post-test was weighed once and required a settling time of 20 min due to the high temperatures involved in the fire conditions. Soot particles in the effluents, created due to the fire conditions were sampled from 30 s before sample exposure to radiant heat, until 30 s after radiant heat source removal. Impact was performed 20 s after time-to-ignition (TTI) and the sample exposure to the heat source was stopped 30 s after flame out (FO). The procedure for capturing particles has been described in previous sections.

## 3.3 | Characterization of particles

Each of the methodologies described in Section 3.2, resulted in particles in either Millipore water / ethanol suspensions or captured on a polycarbonate filter.

### 3.3.1 | Gravimetric analysis

As discussed in details in Section 3.2, each composite sample was weighed prior to and after each test, from

TABLE 2 Details of the test conditions and quantitative analysis of the CF samples (fiber weight fraction =  $69.3 \pm 1.4\%$ , thickness =  $2.31 \pm 0.04$  mm), particles captured during impact and heat/fire tests, and damage area

Heat flux (kW/m <sup>2</sup> )	Impact time (s)	Damage type and area		Total mass loss (mg [%])	Captured in effluents <sup>a</sup> (mg [%])	Captured at back face <sup>a</sup> (mg [%])
		FF (mm <sup>2</sup> )	BF (mm <sup>2</sup> )			
-	0	A/B; $126 \pm 6$	B; $338 \pm 44$	$0.555 \pm 0.045$ / $[0.00185 \pm 0.00015]$	-	$0.176 \pm 0.052$ / $[31.7 \pm 9.3]$
50	90	A; $216 \pm 74$	B; 132	$2056 \pm 379$ / $[6.85 \pm 1.35]$	$0.43 \pm 0.09$ / $[0.021 \pm 0.004]$	-
50	120	D; $258 \pm 80$	D; 323	$2736 \pm 733$ / $[9.05 \pm 2.35]$	-	$5.15 \pm 0.53$ / $[0.18 \pm 0.02]$
50	180	D; $240 \pm 49$	D; 245 $\pm 23$	$2327 \pm 354$ / $[7.8 \pm 1.1]$	-	$4.26 \pm 0.27$ / $[0.18 \pm 0]$
50	240	A/B; 131 $\pm 36$	B; -	$2576 \pm 277$ / $[8.45 \pm 0.85]$	-	$4.55 \pm 0.05$ / $[0.18 \pm 0.002]$
75	TTI <sup>b</sup> +20	A; $126 \pm 10$	-	$6787 \pm 149$ / $[25.8 \pm 0.5]$	$0.795 \pm 0.025$ / $[0.011 \pm 0.0003]$	$3.11 \pm 0.1$ / $[0.05 \pm 0.001]$

Note: A = Dent/depression; B = splits/cracks/fiber breakage; C = split and delamination; D = large cracks with fiber breakage, indentation and penetration. '-' denotes test not performed. Results without standard deviation denote only when one specimen was tested / analyzed.

<sup>a</sup>% captured mass is percentage of total mass loss.

<sup>b</sup>TTI =  $36 \pm 4$  s, FO =  $445 \pm 25$ .

which total mass loss could be recorded and presented in Table 2. Millipore polycarbonate filters from the back face extraction system were also weighed before and after the test from which particles captured from the back face and effluents are tabulated in Table 2. The particles from the front face plate lip and those deposited on the back face chamber that could not be weighed were stored as suspensions for qualitative analysis.

### 3.3.2 | Morphological characterization

For morphological analysis of particles captured on filter papers (in the back surface chamber or in the chimney for effluents),  $1 \times 1$  mm sections of the 47 mm 0.2  $\mu$ m Millipore polycarbonate filter were cut and mounted on SEM stubs.

For particles in Millipore water or ethanol suspensions, droplets of 7.5  $\mu$ L sizes were spread on  $5 \times 7$  mm silicon wafers (sourced from Agar Scientific Ltd), mounted onto SEM stubs and let the water/ethanol evaporate. These wafers reduce interference during SEM, have a surface roughness less than 1 nm and thickness between 460 and 530  $\mu$ m. Scanning Electron Microscopy (SEM) was then performed using either the FEI Quanta 200F instrument at IMT Ales (identified as SEM A: FEI Quanta) or the CARMEN (LNE) platform's Zeiss ULTRA-Plus equipped with a Field Emission Gun (FEG) microscope (identified as SEM B: Zeiss). Post SEM, dimensioning on the particles identified was performed by ImageJ software by manually measuring dimensions (longest diameter or length) of individual resin particles, soot, fibers, composite particles of these components or aggregates / agglomerates, which in some cases resembled small particles.

## 4 | RESULTS AND DISCUSSION

Low velocity impact tests were carried out on samples exposed to different levels of heat exposure using the purpose-built simultaneous impact and heat/fire testing equipment discussed in Section 2, Figure 2. In this horizontal system though, the use of electronic equipment to measure the impact event was not feasible owing to the front and back faces of the samples being enclosed within the particle capturing systems and the high temperatures the composite samples were exposed to during the experiments. Hence, mechanical data such as impactor velocity, force and test time duration for each test could not be recorded. Instead, the focus of this work has been on evaluation of the induced damage area and measurement of the particulates released by low velocity

impact under simultaneous heat/fire. Commonly used damage inspection techniques such as ultrasonic scanning could not be used due to the resin being burnt generating heat/fire damaged sample, hence to determine the type and extent of damage in the CFRP specimens, visual inspection was performed. The effect of impactor shape and geometries were first investigated to determine the optimum type of damage needed to release particulates.

Three impactors as shown in Table 1 were used to impact under different conditions using the methodology presented in Section 3.2 with the exception that in the Advantec filter housing for back face capturing, 47 mm 1.2  $\mu\text{m}$  Whatman micro glass fiber filters were used. The morphologies of the post-impact samples were examined from digital images shown in Figure 4. The gravimetric analysis includes the total mass loss due to the impact and mass captured on the filter in back face chamber (Figure 3E–G, Section 2.2.3).

The small hemispherical impactor (A) penetrated the sample at 23 J (Figure 4A). A large concentration of fine debris and particles was seen on the filter, accounting for 68% of the total mass loss. Damage was concentrated in a small area and this caused the impactor to be retained by the damaged fibers (Figure 4A). Removing the impactor from the sample was difficult and it was likely more damage was caused in this process and extra particles were released.

The flat impactor (B) also penetrated the sample at 22 J (Figure 4B). On reducing impact energy to 16 J, barely visible damage (BVD) was witnessed at the front face and only minor cracks were visible at the back face (Figure 4C). Both tests resulted in effective particle capture ( $>70\%$  of total mass loss).

Use of the hemispherical impactor (C) at 16 J produced BVD at front face and small cracks at the back face (Figure 4D) and fine particles seen at the filter. With 19 J impact energy, visible damage at both front and back faces occurred (Figure 4E) and  $\sim 77\%$  particles were captured at the filter. This is analyzed in more details in the following section.

The effect of impactor shape and geometries is consistent with the damage reported in literature by drop-weight test.<sup>[38–40]</sup> With a conical impactor more energy is absorbed resulting in penetration,<sup>[41]</sup> which was not required in this study, hence not included here. A flat nose impactor (as (B) in Table 1) does not result in total penetration rather induces matrix cracking, delamination and fiber breakage,<sup>[41–43]</sup> as also seen here in Figure 4B. The hemispherical impactors produce the highest contact force when the impact velocities remain below 20 m/s.<sup>[44,45]</sup> The first damage generally occurs in the form of matrix cracking while stress variations

through-thickness results in back-face cracking,<sup>[46]</sup> as seen here in Figure 4E.

After carrying out the provisional tests with the various impactors, hemispherical impactor at 19 J was chosen as it gave the largest amount of fine particles release, which was the primary objective of this study. In these preliminary tests, a glass fiber filter was used for the back face capturing system. It was noted that some particles were entangled in the filter (see Figure 5), hence all further testing was performed with hemispherical impactor at 19 J using polycarbonate filters.

## 4.1 | Low velocity impact: Damage and particle release

In this section the effect of impact and simultaneous heat plus impact on CFRC from a hemispherical impactor of 19 J energy in terms of damage area analysis, quantity (gravimetric analysis) and quality (morphological analysis) of debris released have been discussed. The damage by the impact test was measured manually by sketching around the perimeter of the damage site using Image J analysis software, from which the area of damage could be calculated, the results are given in Table 2. The gravimetric analysis includes the total mass loss due to the impact and heat exposure, the mass captured from sampling of the effluents in the extraction on a filter (setup shown in Figure 3C, Section 2.2.5) and mass captured on the filter in back face chamber (Figure 3E–G, Section 2.2.3). Since mass of individual specimens differed, the total mass loss and captured particles results are also presented as percentage of total initial mass of the sample and the total mass loss, respectively. As noted earlier, the particles remained on the front and back face chambers could not be weighed and were collected as suspension.

Impact on composite sample resulted in an indentation on the front face and two splits, perpendicular to each other on the back face, creating a diamond shape damage area. The damage caused by the out-of-plane impact in this test is typical of carbon fiber composites. The sample had a damage of 126 mm<sup>2</sup> damage area at FF, still had surface indentation, though remained intact (Figure 5A). On the back surface the area is 338 mm<sup>2</sup>. During the impact there is a very small amount of total mass loss ( $\sim 0.002\%$ ). Since the debris was airborne, the total mass loss can be interpreted as released particles,  $\sim 32\%$  of which could be captured on the filter at the back surface. The remaining debris would be on the walls of the front and back face chambers, collected as suspensions. Generally witnessed visually were fine particles on the filter and larger debris remained in the back face chamber and could be seen in the suspension.



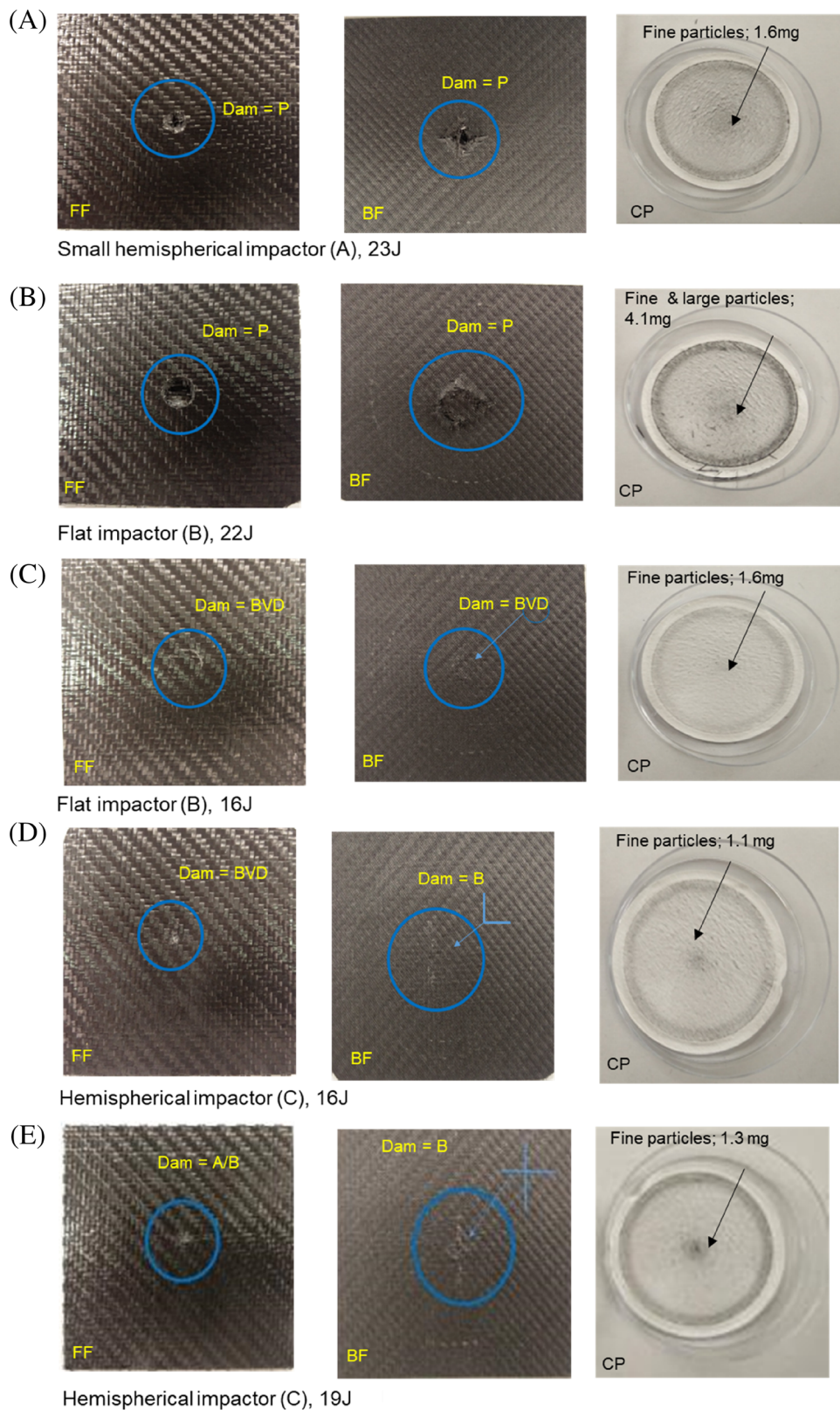


**FIGURE 4** Post impact images of CF samples tested using different impactor types, showing front face (FF), back face (BF) and particles captured on the filter in the BF chamber (CP). Dam = damage type; A = dent/depression; B = splits/cracks/fiber breakage; P = penetration; BVD = barely visible damage

On comparing the particle capture using glass (Figure 4E) or polycarbonate filters (Table 2), it can be seen that % capture is slightly less in latter. In glass fiber filter, some particles were entangled in the fiber, hence the % capture was high,

whereas when polycarbonate filter has negative charge to which positively charged fibers can get stuck, whereas other negative charged or neutral particles may fall off. Hence % particle capture is reduced in the latter.

## 4.2 | Simultaneous heat and impact: Damage and particle release

The conditions used for each test, that is, heat flux and impact time, and the gravimetric results (see above section) for each condition are reported in Table 2. Although it is not possible to determine the mass of released effluents, residue / particles were sampled in selective tests from the extraction chimney. However, the design of the equipment did not allow simultaneous BF and EFF sampling, hence in those tests BF filter could not be used. Moreover, the flow rate for sampling extraction of 1.6 L/s and the main effluents extraction of 24 L/s remains consistent throughout all test conditions, hence the particles captured are indicative of residue and/or soot particles in effluents, not an absolute measurement. These captured particles/soot from effluents have not been analyzed in detail except for gravimetric analysis. For effluents' analysis, a separate set of experiments was performed by modifying the methodology, which will be discussed in a forthcoming publication.

While it was not possible to introduce thermocouples in the tested areas of the composites, the surface temperature was measured with a pyrometer (set at a 350 mm distance) and the temperature versus time curves of all tests are presented in Figure 7.

On exposure to heat at  $50 \text{ kW/m}^2$  for 90 s prior to impact, the damage area increased, the sample had some indentation and minor fiber breakage at the front face and no penetration on the back face. The damage area as well as the amount of damage increased on impact at 120 s, there was penetration through one of the samples. This damage mechanism is very different to impact only, mainly due to the effect of heat on the resin, which undergoes softening followed by decomposition with increased temperature.<sup>[16]</sup> It can be seen from Figure 7 that the surface temperature at 90 s is  $\sim 485^\circ\text{C}$ , however due to short exposure time, the heat transfer through the

thickness would be low, and hence, the resin would have not totally decomposed, leaving some stiffness in the sample resulting in damage on the back surface. On exposure to heat for 120 s, the surface temperature increased to  $\sim 565^\circ\text{C}$ , with more heat transfer, hence increasing damage. However, with increase in impact time to 180 and 240 s, the damaged area reduced, despite penetration in one of samples at 180 s (Figure 6C). A similar decrease in damage has been reported by Im et al.<sup>[25]</sup> As seen from Figure 7, under these conditions the surface temperature after impact suddenly increased by  $\sim 80^\circ\text{C}$ , reaching  $\sim 670^\circ\text{C}$  irrespective of the impact time. This indicates that at and above 180 s the resin throughout the thickness had undergone thermal decomposition, resulting in reduced stiffness of the composite and hence, only indentation damage to samples and reduced fiber breakage. The sudden increase in temperature after impact can be explained through the effect of the simultaneous release and combustion of the volatiles accumulated within the composite layers following decomposition of the resin, as they are forcibly released in a high concentration on impact, resulting in an increase in front face temperature.

As can be seen from Table 2, with impact only there was a minimal mass loss ( $\sim 0.002\%$ ), representing a very small amount of debris/particles released, out of which  $\sim 32\%$  was captured on the filter. On exposure to  $50 \text{ kW/m}^2$  heat flux, the mass loss increased to  $\sim 7\%$ – $9\%$  and it remained similar irrespective of the impact time (90–240 s). In all conditions the mass of particles captured at the back face filter was  $\sim 0.18\%$  of total mass loss. In one of the samples,  $0.021\%$  of the total mass was captured in the effluents. When the sample ignited at  $75 \text{ kW/m}^2$  heat flux, the mass loss increased to  $\sim 26\%$ , as expected. However only  $0.01\%$  was captured in effluents and  $0.05\%$  on the back face filter.

The similar mass loss at all impact conditions (90–240 s, Table 2) and similar mass of captured particles at

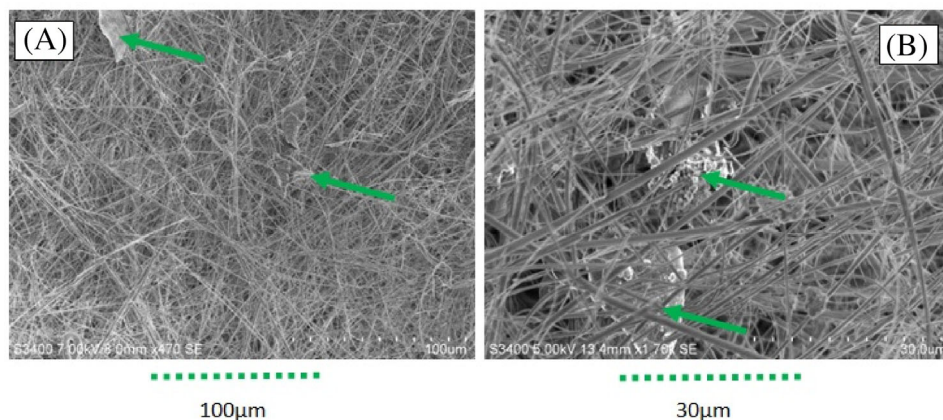


**FIGURE 5** SEM images of Whatman micro glass fiber filter after impact test showing (A), (B) embedded particles between the layers of glass fibers

the back face filters can be explained on the basis that up to 240 s in the absence of ignition, the resin softened, decomposed with some char formation, and releasing very few volatiles, but most of the decomposed resin remained within the composite sample. Resin residue could be seen visually on the walls of the back surface chamber. In all of these there was more debris trapped within decomposed resin residue which adhered on the walls rather than on the filter papers.

#### 4.2.1 | Fire and impact

On exposure to  $75 \text{ kW/m}^2$ , the sample self-ignited at  $36 \pm 5 \text{ s}$ , the temperature increased rapidly to  $840^\circ\text{C}$  within 80 s as can be seen from Figure 7. Under these conditions, a high percentage of the epoxy matrix and possibly some fiber sizing were decomposed, becoming residual char, soot or volatiles, explaining  $\sim 26\%$  mass loss (Table 2). Impact was performed 20 s after sample ignition to ensure ignition in all specimens, and that the samples would have some residual mechanical integrity. The damage witnessed was minimal on samples (Figure 6F) with front face indentation and some fiber breakage, which was expected due to loss of stiffness.

### 4.3 | Qualitative analysis of released particles

As described in Section 3.3.2,  $1 \times 1 \text{ mm}$  sections of the Millipore polycarbonate filters from back face (BF) chamber, where particles were deposited directly during the experiment, and silicon wafers, prepared by depositing suspensions from back face (BF) and front

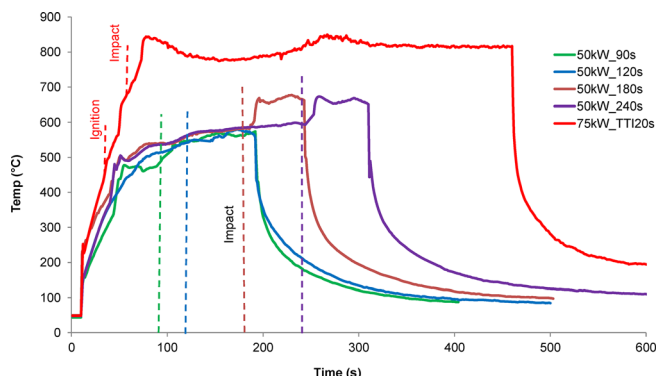


**FIGURE 7** Temperature–time curves measured at the front surfaces of the carbon–epoxy composite laminates when exposed to the heat flux of 50 or  $75 \text{ kW/m}^2$ . The times at which different samples were impacted are represented by vertical lines

face (FF) were examined by SEM. Manual measurements of dimensions (longest diameter or length) of resin particles, soot and fibers were performed using ImageJ software and the results are presented in Table 3.

#### 4.3.1 | Impact only

In general, the particles released during impact only were fibers, fibers with resin particles attached and individual resin particles (Figure 8). On the BF filter the length and diameter of 55 fibers (Figure 8A) were measured that ranged from 10.4 to  $140.4 \mu\text{m}$  and 6.4 to  $18.8 \mu\text{m}$  respectively (Table 3). The virgin fiber diameter of TORAYCA T300 is  $7 \mu\text{m}$ . On the majority of the fibers observed, a thin layer of epoxy resin was present and on few fibers some resin particles. Many resin particles were observed on the filter, the range of these particles was  $0.26\text{--}54 \mu\text{m}$ . In addition, a low concentration of resin particles was also observed in both BF and FF suspensions which ranged between  $0.6\text{--}49.2 \mu\text{m}$  and  $5.2\text{--}81.5 \mu\text{m}$  respectively (Figure 8B,C).

#### 4.3.2 | Heat and impact

On exposure to simultaneous heat and impact at different times, resin particles on the BF filter generally appeared similar to those observed during impact only, with few particles that also appeared to be starting to decompose into smaller particles (Figure 9A–C) or in some cases starting to agglomerate (Figure 9B). Some resin particles were fiber shaped, but fibers were not observed. The resin particle size was higher until exposure to heat and 120 s impact time compared to the impact only condition, which could be due to the semi-decomposed resin being less brittle, so harder to break into very small size pieces. With increase in impact time, the size of the resin particles decreased from 2.2 to  $53 \mu\text{m}$  at 120 s and 0.12 to  $13 \mu\text{m}$  at 240 s (Table 3). Comparing the resin particles sampled on the BF filters during impact at 180 s and 240 s, the smallest resin particles measured show a decrease to  $0.12 \mu\text{m}$  compared to  $0.26 \mu\text{m}$  (Table 3) for impact only. Impact at 120 s showed an increase, however, this condition had the smallest sample set size. As mentioned earlier, no BF filter was used for sampling during impact at 90 s as, particles were sampled in the effluents, and effluent and BF filter sampling could not be done simultaneously. The purpose of the impact at 90 s test was to check for fibers / particles present in the effluents during the peak smoke production which occurred  $\sim 90 \text{ s}$  after sample exposure to radiant heat. However, particulates/fibers capture and analysis from the effluents' required a separate set of experiments,



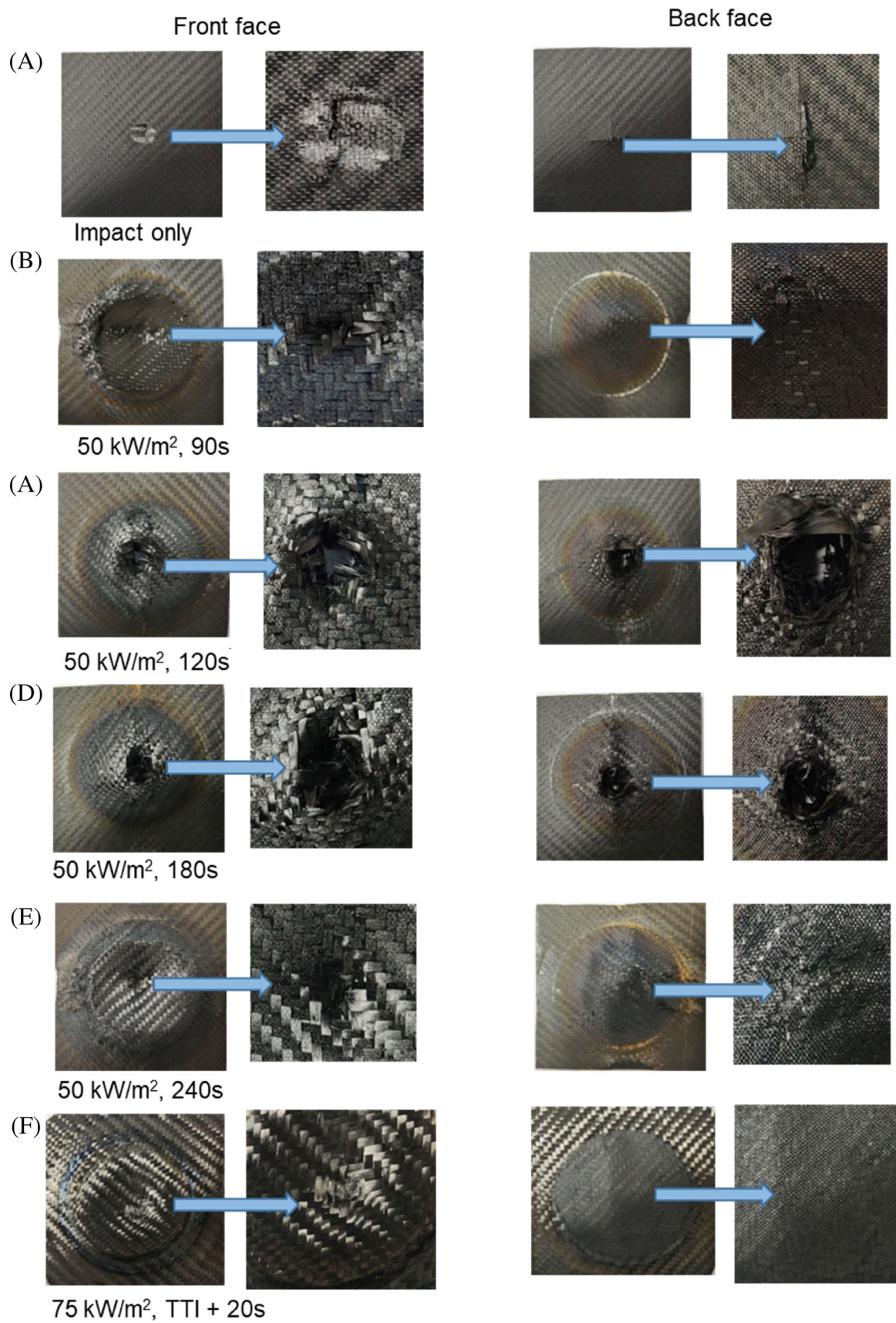


FIGURE 6 Post impact images of all tested samples

which were performed by modifying the methodology, and will be discussed in a forthcoming publication.

From the BF suspensions, while some particles seen were similar to those on the filter including some fibers (Figure 9E), at higher impact time most of the resin was decomposed, indicating that any undecomposed / semi-decomposed particles were mainly captured on the filter paper and decomposed resin adhered to the walls.

In the FF suspension, some ultrafine particles (0.07  $\mu\text{m}$  diameter) (Table 3) were observed, the particle size though ranged from 0.07  $\mu\text{m}$  to 123  $\mu\text{m}$  for 120 s and 180 s. At 240 s impact time particle size increased slightly to 0.17  $\mu\text{m}$  (Table 3) and some fibers were also observed as can be seen from Figure 9F. The fiber diameter was 7.4–9.0  $\mu\text{m}$ , indicating that these have not been exposed to heat for long enough time for the sizing to be removed and undergo oxidation and hence, no reduction in diameter.

#### 4.3.3 | Fire and impact

On exposure to 75 kW/m<sup>2</sup> and impacting 20 s after the ignition, fibers, particles and soot particles were captured.

#### Fibers

Fibers in many forms were observed during fire conditions. Resin coated fibers; a fiber where the sizing had decomposed, and the individual fibrils could be viewed; a damaged fiber where it appeared fibril fragments had been released; and fibril bundles were all observed (Figure 10A–C). The resin coated fibers had lengths between 9.1 and 246.6  $\mu\text{m}$  (Table 3) and diameters 7.4–9  $\mu\text{m}$  (Table 3), they were observed both on the BF filter and in the BF suspension. The decomposed fiber was observed in the BF suspension and had a reduced diameter of 3.7  $\mu\text{m}$  (Figure 10D). Finally, also observed in the BF suspension were the fibril bundles (Figure 10D). Of the fibril diameters, 42 measurements resulted in a range of 0.089–0.7  $\mu\text{m}$ . Some measurements of the lengths were also possible, and the range was 5.4–20.6  $\mu\text{m}$ . Multiple bundles were seen during SEM, which indicated that this was not a random event.

#### Resin particles

Resin Particles were observed in both BF filter (Figure 10A,D,E) and suspension, and in FF suspension, they ranged in diameter between 0.23–70  $\mu\text{m}$ ,

**TABLE 3** Particle size distribution for the particles captured during impact and heat, fire tests.

Condition	Particle types	Particles from BF				Particles from FF suspension	
		Filter		Suspension			
		No.	Size ( $\mu\text{m}$ )	No.	Size ( $\mu\text{m}$ )	No.	Size ( $\mu\text{m}$ )
Impact only	Fibers	57	L = 10.4–140 D = 6.4–18.8				
	RP	720	0.26–54	14	0.6–49.2	13	5.2–81.5
50 kW/m <sup>2</sup> / Impact at 90 s	RP	4	6–16.5	26	2.7–40	1250	1–155.4
	Spheres	62	0.3–7.1	-	-	-	-
50 kW/m <sup>2</sup> / Impact at 120 s	RP	19	2.3–52.5	-	-	2051	0.07–122.7
50 kW/m <sup>2</sup> / Impact at 180 s	RP	157	0.12–34.8	-	-	542	0.06–112.1
50 kW/m <sup>2</sup> / Impact at 240 s	Fibers	4	L = 26–280 D = 7.2–9.9	-	-	-	-
	RP	26	0.13–13	-	-	774	0.17–196.2
75 kW/m <sup>2</sup> / Impact at TTI + 20 s	Fibers	5	L = 9.1–247 D = 7.4–9	3	L = 44.2–198	-	-
				4	D = 7–8.2		
	Decomposed fiber	-	-	1	D = 3.7	-	-
	Fibrils	-	-	13	L = 5.4–20.7	-	-
				42	D = 0.089–0.7		
	RP	120	0.23–69.8	26	0.87–47.1	235	0.08–192
	Soot	-	-	30	0.05–0.36	316	0.05–0.36

Note: No. = number of particles for measurements; L = length; D = Diameter.

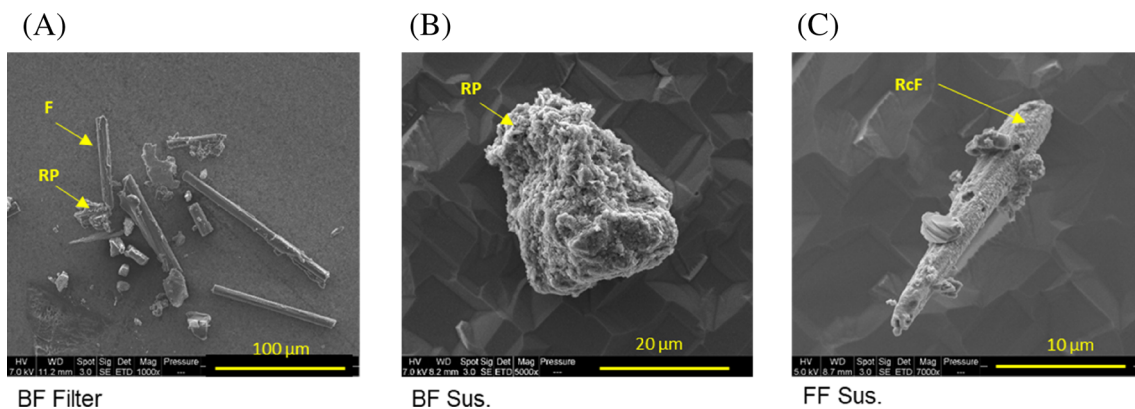


**FIGURE 8** SEM (A: FEI quanta) images of particles (fibers (F), resin particles (RP) and resin coated fibers (RcF) decomposed resin fragment (RP)) captured from impact test: (A) BF filter, (B) BF suspension and (C) FF suspension

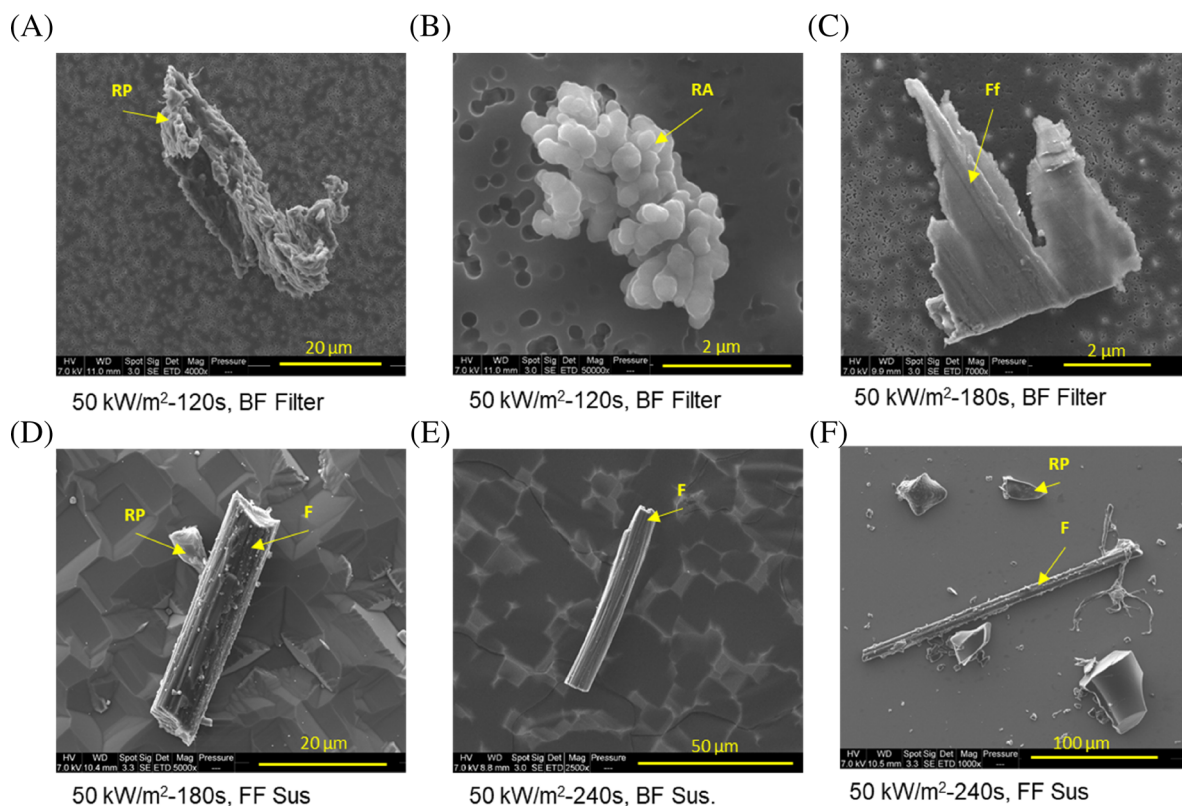


**FIGURE 9** SEM (A: FEI quanta) images of particles (fibers (F), fiber fragment (FF) resin particles (RP), resin agglomerate (RA)) captured from 50 kW/m<sup>2</sup> heat exposure and different impact times as: (A),(B) 120 s, BF filter; (C) 180 s, BF filter; (D) 180 s, FF suspension; (E) 240 s, BF suspension and (F) 240 s, FF suspension

0.87–47 μm and 0.08–192 μm, respectively (Table 3). Some of the particles appeared similar to those observed in impact only and heat plus impact conditions. However, there were also many decomposed, some heavily, particles or particle agglomerates. Some of the heavily decomposed particles resembled soot, but were more porous than soot agglomerates, probably

formed during partial melting after the loss of resin's crosslinked structure.

#### Soot

Soot agglomerates, formed following nucleation / growth process from aromatic precursors found in decomposition gasses, were observed in FF suspension. These were



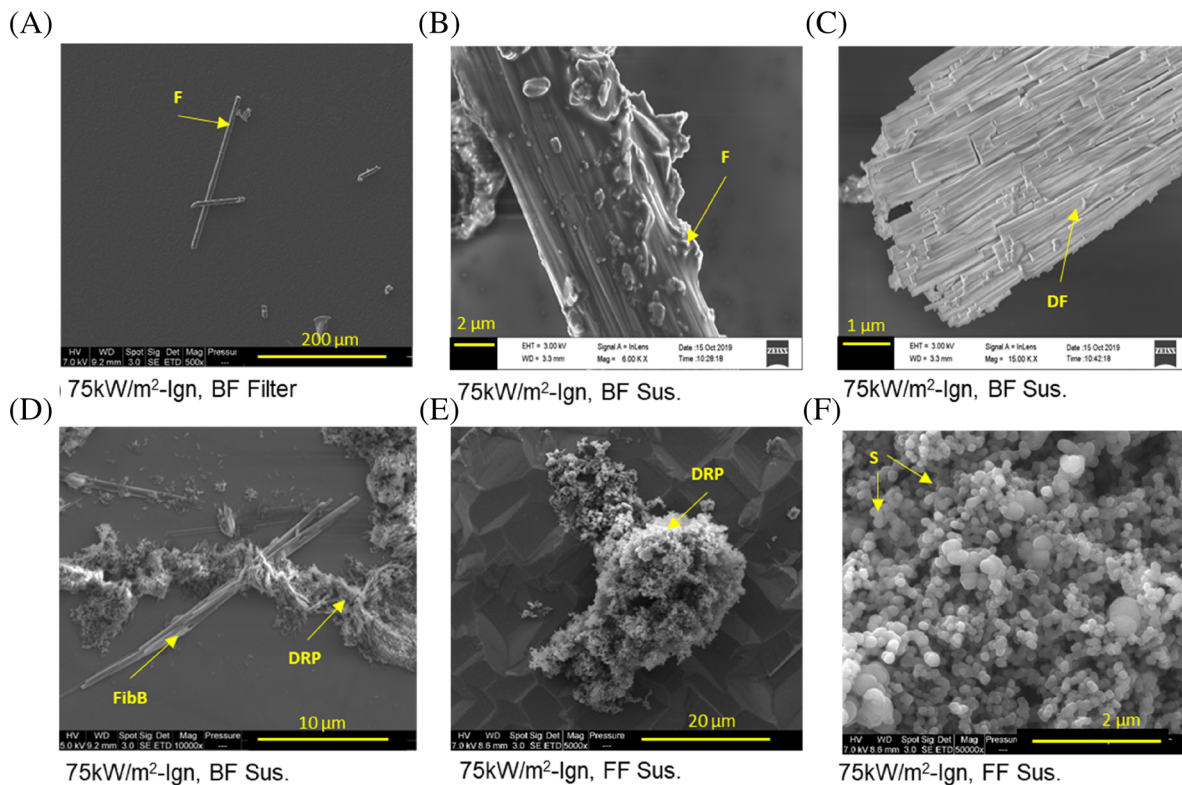


**FIGURE 10** SEM (A: FEI quanta (A),(D)–(F) and B: Zeiss (B),(C)) images of particles (fibers (F), decomposed fiber (DF), fibril bundle (FibB), resin particles (RP), decomposed resin particles (DRP) and soot (S)) captured from 75 kW/m<sup>2</sup> heat exposure and impact at TTI + 20 s as: (A) BF filter; (B)–(D) BF suspension (BF Sus); (E),(F) FF suspension (FF Sus)

measured and were in the range 0.07–0.44 µm, (Table 3). Although many of the measurements were of the primary soot particles within the agglomerates, individual soot released from the agglomerate was also observed under high magnification.

## 5 | CONCLUSIONS

A novel laboratory scale testing equipment capable of capturing particles released from carbon fiber composites during simultaneous exposure to combinations of heat or fire, and impact conditions not previously reported in detail has been developed. This purpose built equipment consists of a cone calorimeter heater and a pendulum impactor. An experimental protocol to capture particles, and for characterization of the captured particles has been presented. The composite samples were exposed to 50 and 75 kW/m<sup>2</sup> for a range of time intervals prior to impact in order to study the effect of impact on samples following varying degrees of thermal decomposition and combustion. A good repeatability of the test results has been obtained. A range of particulates including broken carbon fibers, resin particles and resin coated carbon fibers were all observed in the debris captured on the back face filter or collected in the back and front face chambers. During heat and impact conditions

there were largely similar observations, but the resin was more decomposed, particularly at higher times to impact. The particle sizes reduced with increasing time up to 180 s prior to impact, after which the size increased, probably due to agglomeration/aggregation of the decomposed resin. In the case of fire and impact much smaller carbon fibers/fibrils were captured on the front and back faces. To conclude, this study has demonstrated the development of novel equipment and methodology needed to provide the key data essential for the future health and safety risk assessment in combination with particulate toxicity data. This toxicity data has also been derived, and the toxicity evaluation will be presented in our forthcoming publication.

## ACKNOWLEDGMENTS

The authors acknowledge the Defence Science and Technology Laboratory (Dstl), UK for the financial and technical assistance. Bitrez Ltd. UK is acknowledged for supply of the resin. Technical support from J. Milnes from Bolton during equipment designing; J-C Roux from IMT Ales for SEM study; F. De Lagos from LNE during equipment setup is much appreciated.

## ORCID

Baljinder K. Kandola  <https://orcid.org/0000-0002-3621-3724>

Peter Myler  <https://orcid.org/0000-0003-3611-1979>  
 Laurent Ferry  <https://orcid.org/0000-0002-1558-0082>  
 José-Marie Lopez-Cuesta  <https://orcid.org/0000-0002-1723-3287>  
 Carine Chivas-Joly  <https://orcid.org/0000-0002-3927-8275>

## REFERENCES

- [1] J. Leng, T. Guo, M. Yang, Z. Guo, Z. Fang, Z. Liu, D. Li, D. Sun, *Materials* **2020**, *13*, 187. <https://doi.org/10.3390/ma13010187>
- [2] N. Hongkarnjanakul, C. Bouvet, S. Rivallant, *Compos. Struct.* **2013**, *106*, 549.
- [3] M. Bulut, A. Erklig, E. Yeter, *Compos. Part B Eng.* **2016**, *98*, 9.
- [4] S. Abrate, *Impact on composite structures*, Cambridge University Press, Cambridge, UK **1998**.
- [5] M. N. Ghasemi Nejhad, A. Parvizi-Majidi, *Composites* **1990**, *21*(2), 155.
- [6] B. Vieille, V. M. Casado, C. Bouvet, *Compos. Struct.* **2013**, *101*, 9.
- [7] B. Vieille, V. M. Casado, C. Bouvet, *Compos. Struct.* **2014**, *110*, 207.
- [8] O. Ishai, A. Shragai, *Compos. Struct.* **1990**, *14*(4), 319. [https://doi.org/10.1016/0263-8223\(90\)90013-5](https://doi.org/10.1016/0263-8223(90)90013-5)
- [9] S. K. Bhudolia, S. C. Joshi, *Compos. Struct.* **2018**, *203*, 696.
- [10] E. A. Abdallah, C. Bouvet, S. Rivallant, B. Broll, J.-J. Barrau, *Compos. Sci. Technol.* **2009**, *69*(7), 1238.
- [11] M. O. W. Richardson, M. J. Wisheart, *Compos. Part A* **1996**, *27*(12), 1123.
- [12] A. Riccio, A. De Luca, G. Di Felice, F. Caputo, *Compos. Part B* **2014**, *66*, 340.
- [13] U. Farooq, P. Myler, *Acta Astronaut.* **2014**, *102*, 169.
- [14] S. Abrate, *Compos. Struct.* **2001**, *51*, 129.
- [15] Y. Shi, T. Swait, C. Soutis, *Compos. Struct.* **2012**, *94*, 2902.
- [16] C. Katsoulis, B. K. Kandola, P. Myler, E. Kandare, *Compos. Part A* **2012**, *43*, 1389.
- [17] E. Kandare, B. K. Kandola, P. Myler, G. Edwards, *J. Compos. Mater.* **2010**, *44*, 3093.
- [18] E. Kandare, B. K. Kandola, E. D. McCarthy, P. Myler, G. Edwards, J. F. Yuan, Y. C. Wang, *J. Compos. Mater.* **2011**, *45*, 1511.
- [19] C. P. Gardiner, Z. Mathys, A. P. Mouritz, *Appl. Compos. Mater.* **2002**, *9*, 353.
- [20] A. P. Mouritz, C. P. Gardiner, *Compos. Part A* **2002**, *33*, 609.
- [21] C. A. Ulven, U. K. Vaidya, *Compos. Part A* **2006**, *37*, 997.
- [22] B. Kandola, E. Kandare, Composites having improved fire resistance. in *Advances in fire retardant materials* (Eds: A. R. Horrocks, D. Price), Woodhead Publishing Ltd, Cambridge **2008**, Chapter 15, p. 398. <https://doi.org/10.1533/9781845694701.3.398>
- [23] A. P. Mouritz, A. G. Gibson, *Fire properties of polymer composite materials*, Dordrecht, Springer-Verlag, New York **2006**, p. 359.
- [24] P. N. B. Reis, J. A. M. Ferreira, Z. Y. Zhang, T. Benameur, M. O. W. Richardson, *Compos. Part B* **2014**, *56*, 290. <https://doi.org/10.1016/j.compositesb.2013.08.048>
- [25] K.-H. Im, C.-S. Cha, S.-K. Kim, I.-Y. Yang, *Compos. Part B* **2001**, *32*(8), 669.
- [26] G. A. Bibo, D. Leicy, P. J. Hogg, M. Kemp, *Composites* **1994**, *25*(6), 414.
- [27] B. K. Kandola, A. R. Horrocks, M. R. Rashid, Effect of reinforcing element on burning behaviour of fibre-reinforced epoxy composites. in *Recent advances of flame retardancy of polymeric materials. Proceedings of the 17th conference* (Ed: M. Lewin), Business Communication Company, Stamford, Connecticut **2006**.
- [28] S. Feih, A. Mouritz, *Compos. A: Appl. Sci. Manuf.* **2012**, *43*(5), 765.
- [29] Y. Yin, J. G. P. Binner, T. E. Cross, S. J. Marshall, *J. Mater. Sci.* **1994**, *29*, 2250.
- [30] G. La Delfa, J. W. Luinge, A. G. Gibson, *Plast. Rubber Compos.* **2009**, *38*(2–4), 111. <https://doi.org/10.1179/174328909x387900>
- [31] T. Hertzberg, *Fire Mater.* **2005**, *29*(4), 231. <https://doi.org/10.1002/fam.882>
- [32] J. Costantino, J. J. Jarbeau, T. J. Hintz, M. Hinojosa, C. W. Edwards, T. W. Batten, J. E. Black. Composite material hazard assessment at crash sites. Wright-Patterson AFB, OH 45433–7913: Air Force Research Laboratory, 2001. Report updated, AFRL-SA-WP-SR-2015–0011, 2015.
- [33] S. Gandhi, R. Lyon, L. Speitel, *J. Fire Sci.* **1999**, *17*(1), 20. <https://doi.org/10.1177/073490419901700102>
- [34] V. L. Bell. Sources of released carbon fibres. NASA Langley Research Centre, CP2074, **1974**.
- [35] E. L. Morrey Potential hazards associated with combustion of polymer composite materials, and strategies for their mitigation. PhD Thesis., Centre for Composite Materials, Imperial College of Science, Technology & Medicine, London, UK, 2001.
- [36] ISO 5660-1:1993. Fire tests on building materials and structures–Part 15: Method for measuring the rate of heat release of products
- [37] ASTM D7136 / D7136M–20, *Standard Test Method for Measuring the Damage Resistance of a Fiber-Reinforced Polymer Matrix Composite to a Drop-Weight Impact Event*, ASTM International, West Conshohocken, PA **2020** [www.astm.org](http://www.astm.org)
- [38] R. A. James. Impact damage resistance and damage tolerance of fibre reinforced laminated composites, PhD thesis, University of Bolton, UK. **2006**.
- [39] T. Mitrevski, I. H. Marshall, R. S. Thomson, R. Jones, *Compos. Struct.* **2006**, *76*, 209.
- [40] S. Ercan, L. Benjamin, D. Feridun, *Mater. Des.* **2013**, *52*, 67.
- [41] Y. Deng, W. Zhang, Z. Cao, *Mater. Des.* **2012**, *41*, 266.
- [42] C. S. Lopes, *Part I. Exp. Compos Sci Technol* **2009**, *69*(7–8), 926.
- [43] U. Farooq, M. P. Peter, *Acta Astronaut.* **2015**, *115*, 314.
- [44] Y. O. Kas, C. Kaynak, *Polym. Test.* **2004**, *24*, 114.
- [45] F. J. Yang, W. J. Cantwell, *Compos. Sci. Technol.* **2010**, *70*(2), 336.
- [46] U. Polimeno, M. Michele, D. P. Almond, S. L. Angioni, *Appl. Compos. Mater.* **2010**, *17*, 481.